Low temperature heat capacity of Na 4 UO 5 and Na 4 NpO 5

A.L. Smith, J.-C Griveau, E Colineau, P. E. Raison, G Wallez, R.J.M. Konings

J. Chem. Thermodynamics 91 (2015) 245–255

Contents lists available at ScienceDirect

J. Chem. Thermodynamics

journal homepage: www.elsevier.com/locate/jct

Low temperature heat capacity of Na_4UO_5 and Na_4NpO_5

A.L. Smith [a,b,*], J.-C. Griveau [a], E. Colineau [a], P.E. Raison [a], G. Wallez [c,d], R.J.M. Konings [a,*]

[a] European Commission, Joint Research Centre, Institute for Transuranium Elements, P.O. Box 2340, D-76125 Karlsruhe, Germany
[b] Department of Materials Science and Metallurgy, University of Cambridge, 27 Charles Babbage Road, Cambridge CB3 0FS, United Kingdom
[c] PSL Research University, Chimie ParisTech-CNRS, Institut de Recherche de Chimie Paris, 75005 Paris, France
[d] Sorbonne University, UPMC Université Paris 06, 75005 Paris, France

ARTICLE INFO

Article history:
Received 20 March 2015
Received in revised form 29 July 2015
Accepted 1 August 2015
Available online 7 August 2015

Keywords:
Heat capacity
Entropy
Calorimetry
Sodium uranates
Sodium neptunates

ABSTRACT

The low temperature heat capacities of Na_4UO_5 and Na_4NpO_5 have been measured for the first time in the temperature range (1.9 to 292) K using a Quantum Design PPMS (Physical Property Measurement System) calorimeter. The experimental data have been fitted to theoretical functions below 20 K, and to a combination of Debye and Einstein functions above this temperature. The heat capacity and entropy values at $T = 298.15$ K have been derived as $C^o_{p,m}(Na_4UO_5, cr, 298.15\ K) = (220.6 \pm 6.7)\ J \cdot K^{-1} \cdot mol^{-1}$, $S^o_m(Na_4UO_5, cr, 298.15\ K) = (247.5 \pm 6.2)\ J \cdot K^{-1} \cdot mol^{-1}$, $C^o_{p,m}(Na_4NpO_5, cr, 298.15\ K) = (219.0 \pm 6.6)\ J \cdot K^{-1} \cdot mol^{-1}$, and $S^o_m(Na_4NpO_5, cr, 298.15\ K) = (247.5 \pm 6.2)\ J \cdot K^{-1} \cdot mol^{-1}$. When combined with the enthalpies of formation reported in the literature, these data yield standard entropies and Gibbs energies of formation as $\Delta_f S^o_m(Na_4UO_5, cr, 298.15\ K) = -(520.8 \pm 6.3)\ J \cdot K^{-1} \cdot mol^{-1}$, $\Delta_f S^o_m(Na_4NpO_5, cr, 298.15\ K) = -(521.0 \pm 6.3)\ J \cdot K^{-1} \cdot mol^{-1}$, $\Delta_f G^o_m(Na_4UO_5, cr, 298.15\ K) = -(2301.7 \pm 2.9)\ kJ \cdot mol^{-1}$ and $\Delta_f G^o_m(Na_4NpO_5, cr, 298.15\ K) = -(2159.7 \pm 6.0)\ kJ \cdot mol^{-1}$.

1. Introduction

In the potential event of a breach of the stainless steel cladding in a Sodium-cooled Fast Reactor (SFR), the sodium metallic coolant could come into contact with the nuclear fuel. $(U,Pu)O_2$ mixed oxide fuel is the preferred option for SFRs because of the long experience accumulated with the current second generation Light Water reactor systems in terms of fabrication, reactor operation, reprocessing, and risk assessment. The additional incorporation of minor actinides (Np,Am,Cm) into the fuel is moreover envisioned in the framework of the international Generation IV program so as to reduce the radiotoxic inventory of the fuel cycle and its long term impact [1,2]. One solution to reduce the amount of waste and its radiotoxicity is indeed to recover the long-lived isotopes from the spent fuel and re-irradiate them in a fast reactor to transmute them into radioactive elements with shorter half-lives [1,2]. In this respect, the development of the SFR concept has led to a considerable interest for the reaction products between sodium coolant and $(U,Pu,Np)O_2$ nuclear fuel. A thorough knowledge of their structural and thermodynamic properties is essential from a safety perspective.

The phases forming in the (Na + U + O), (Na + Np + O), and (Na + Pu + O) systems are numerous: tetravalent Na_2PuO_3, pentavalent $NaUO_3$, Na_3AnO_4, Na_5PuO_5, hexavalent Na_2UO_4, Na_2NpO_4, Na_4AnO_5, $Na_2An_2O_7$, and heptavalent Na_5NpO_6, Na_5PuO_6 (An = U, Np,Pu) [3–13]. The structural properties of the sodium uranium ternary oxides have been reviewed extensively [3–6,8]. Their thermodynamic functions are also fairly well established at $T = 298.15$ K [14,15]. Only the heat capacities, entropies, and Gibbs energies of Na_4UO_5 and β-Na_2UO_4 are missing. By contrast, there is little knowledge of the sodium neptunates and plutonates. Keller et al. [9,10,16], Pillon et al. [17,4], Kleykamp [18], Smith et al. [11,13], and Bykov et al. [12] have contributed to their structural characterization, but there is a real lack of thermodynamic information on these phases [15]. Only the enthalpies of formation at $T = 298.15$ K of α-Na_2NpO_4, β-Na_2NpO_4, Na_4NpO_5, and $Na_2Np_2O_7$ have been measured experimentally using solution calorimetry [19,20,15] and Knudsen effusion mass spectrometry [21]. To complete the data on the (Na + U + O) and (Na + Np + O) systems, we report for the first time low temperature heat capacity measurements on Na_4UO_5 and Na_4NpO_5 and the determination of their heat capacities, entropies and Gibbs energies at $T = 298.15$ K.

* Corresponding authors at: European Commission, Joint Research Centre, Institute for Transuranium Elements, P.O. Box 2340, D-76125 Karlsruhe, Germany.
E-mail addresses: als77@cantab.net (A.L. Smith), rudy.konings@ec.europa.eu (R.J.M. Konings).

http://dx.doi.org/10.1016/j.jct.2015.08.003
0021-9614/

2. Experimental methods

2.1. Sample preparation and characterization

The Na_4UO_5 material was kindly provided by NRG (Nuclear Research & Consultancy Group, Petten, The Netherlands). The sample as received was furthermore sintered at $T = 923$ K under oxygen flow for 12 h to produce a compact material suited for the measurements.

Na_4NpO_5 was synthesized under oxygen flow by reaction at $T = 1100$ K between accurately weighted samples of neptunium dioxide ($^{237}NpO_2$ from ORNL, Oak Ridge National Laboratory) and sodium carbonate (Na_2CO_3 99.95%, Sigma). The total heating time amounted to 70 h, with intermediate regrinding steps. The purity of the samples was examined by X-ray diffraction at room temperature and ICP-MS analysis.

The X-ray diffraction measurements were carried out using a Bruker D8 X-ray diffractometer mounted in the Bragg–Brentano configuration with a curved Ge monochromator (1 1 1), a ceramic copper tube (40 kV, 40 mA), and equipped with a LinxEye position sensitive detector. The data were collected at room temperature, i.e. 300(5) K, by step scanning in the angle range $10° \leqslant 2\theta \leqslant 120°$, with an integration time of about 8 h, a count step of 0.02° (2θ), and a dwell of 5 s/step. Structural analysis was performed by the Rietveld method with the Fullprof2k suite [22].

Na_4UO_5 and Na_4NpO_5 are isostructural and crystallize in the tetragonal space group $I4/m$ ($Z = 2$) [7,13]. The lattice parameters found in the present work, $a = 0.7549(3)$ nm, $c = 0.4637(3)$ nm for Na_4UO_5 (Vol. = 0.2643(2) nm^3 and $\rho = 5.152(4)\ g \cdot cm^{-3}$), and $a = 0.7533(3)$ nm, $c = 0.4615(3)$ nm for Na_4NpO_5 (Vol. = 0.2619(2) nm^3 and $\rho = 5.199(4)\ g \cdot cm^{-3}$), respectively, are in very good agreement with the values reported in the literature [7,13]. Some very minor secondary phases of α-Na_2UO_4 and α-Na_2NpO_4 were detected with X-rays and quantified using the Rietveld method and ICP-MS analysis. According to our Rietveld refinement, the Na_4UO_5 batch was pure at 98.4 wt% with 1.6 wt% α-Na_2UO_4 impurity, corresponding to the composition $Na_{3.962}UO_{4.981}$. The ICP-MS analysis yielded a sodium to uranium ratio of (3.963 ± 0.016) at/at,[1] in very good agreement with the latter quantification. The Na_4NpO_5 batch was pure at 99.5 wt% with 0.5 wt% α-Na_2NpO_4 impurity, corresponding to the composition $Na_{3.988}NpO_{4.982}$. The ICP-MS analysis yielded a sodium to neptunium ratio of (4.006 ± 0.048) at/at[1], also in good agreement with the quantification using X-rays.

2.2. Heat capacity measurements

Low temperature heat capacity measurements were performed in the temperature ranges (1.9 to 288.7) K and (2.4 to 292.2) K for Na_4UO_5 and Na_4NpO_5, respectively, using a PPMS (Physical Property Measurement System, Quantum Design) instrument in the absence of a magnetic field. This technique is based on a thermal relaxation method, which was critically assessed by Lashley et al. [23]. The measurements were carried out on pellets of 28.90(5) mg of Na_4UO_5 and 21.07(5) mg of Na_4NpO_5 materials encapsulated in Stycast 2850 FT, and the heat capacity contribution of the Stycast was subtracted from the recorded data. A more detailed description of the experimental procedure, which is particularly well adapted to the study of radioactive materials, was given in [24]. The contribution of the sample platform, wires, and grease was also deduced by a separate measurement of an addenda curve. The collected data for Na_4UO_5 and Na_4NpO_5 were finally corrected for 1.6 wt% and 0.5 wt% impurities of α-Na_2UO_4 and α-Na_2NpO_4, respectively, which were measured by Osborne et al. [25] and Smith et al. [26].

Considering the accuracy of the PPMS instrument as estimated by Lashley et al. [23], the reproducibility of the measurements, and the error introduced by the encapsulation procedure in Stycast of these radioactive materials [24], the final uncertainty was estimated at about (1 to 2)% in the middle range of acquisition $T =$ (10 to 100) K, and reaching about 3% at the lowest temperatures and near room temperature. The use of Stycast is the main contributor to the combined standard uncertainties on the heat capacities and entropies quoted hereafter. The uncertainties introduced by the presence of impurities are moreover within the uncertainty range of the method.

3. Results

The experimental heat capacity data collected for both samples in the absence of a magnetic field are shown in figure 1 and 2, and listed in table 8 and 9, respectively. As the temperature approaches 298.15 K, the specific heat reaches in both cases values that are about $30\ J \cdot K^{-1} \cdot mol^{-1}$ below the classical Dulong–Petit limit ($C_{lat} = 30R \approx 249\ J \cdot K^{-1} \cdot mol^{-1}$ for the ten atoms in the formula unit).

The heat capacity of Na_4UO_5 increases smoothly with temperature. Interestingly, the low-temperature heat capacity of Na_4NpO_5 shows a broad anomaly between $T = (3$ and $15)$ K with a maximum at about $T = 7$ K. This anomaly was found to be slightly shifted to lower temperatures when a magnetic field is applied as reported in our previous work [13]. The hypothesis of a magnetic ordering transition at about $T = 7$ K was ruled out based on our Mössbauer spectroscopy and magnetic susceptibility results. Instead, this feature was interpreted as a Schottky-type anomaly associated with low-lying electronic energy levels. Its entropy contribution was moreover estimated as $4.57\ J \cdot K^{-1}\ mol^{-1}$ after subtraction of the lattice contribution approximated with that of Na_4UO_5 [13]. We refer the reader to [13] for further details on this particular feature, and derivation of its associated entropy contribution.

In the present work, the thermodynamic functions of Na_4UO_5 and Na_4NpO_5 were derived at $T = 298.15$ K by fitting the experimental data to theoretical functions below $T = (20.0$ and $4.3)$ K [27], respectively, and a combination of Debye and Einstein heat capacity functions [28–30] from $T = (20.0$ to $288.7)$ K and $T = (23.2$ to $292.2)$ K, respectively. In addition, the Schottky anomaly observed for the neptunium compound was fitted between $T = (4.3$ and $23.2)$ K with a series of cubic spline polynomial functions. The fitted data are shown with solid lines in Figs. 1–3.

The heat capacity values at $T = 298.15$ K were obtained by extrapolation, yielding $C^o_{p,m}(Na_4UO_5, cr, 298.15\ K) = (220.6 \pm 6.7)$[2] $J \cdot K^{-1} \cdot mol^{-1}$ and $C^o_{p,m}(Na_4NpO_5, cr, 298.15\ K) = (219.0 \pm 6.6)$[3] $J \cdot K^{-1} \cdot mol^{-1}$, respectively. The experimental standard entropies at $T = 298.15$ K were determined by numerical integration of $(C_{p,m}/T) = f(T)$ using the aforementioned fitted functions, yielding $S^o_m(Na_4UO_5, cr, 298.15\ K) = (247.5 \pm 6.2)\ J \cdot K^{-1} \cdot mol^{-1}$ and $S^o_m(Na_4\ NpO_5, cr, 298.15\ K) = (247.5 \pm 6.2)\ J \cdot K^{-1} \cdot mol^{-1}$, respectively. Finally, standard thermodynamic functions were calculated at selected temperatures between (0 and 300) K and are listed in tables 10 and 11.

[1] The uncertainty is an expanded uncertainty $U = k.u_c$ where u_c is the combined standard uncertainty estimated following the ISO/BIPM Guide to the Expression of Uncertainty in Measurement. The coverage factor is $k = 2$.

[2] The encapsulation procedure in Stycast is the main contributor (3%) to the quoted combined standard uncertainty. The errors associated with the Debye and Einstein fit (0.4%) and impurity contamination (0.4%) contribute very little to the final uncertainty.

[3] The encapsulation procedure in Stycast is the main contributor (3%) to the quoted combined standard uncertainty. The errors associated with the Debye and Einstein fit (0.4%) and impurity contamination (0.1%) contribute very little to the final uncertainty.

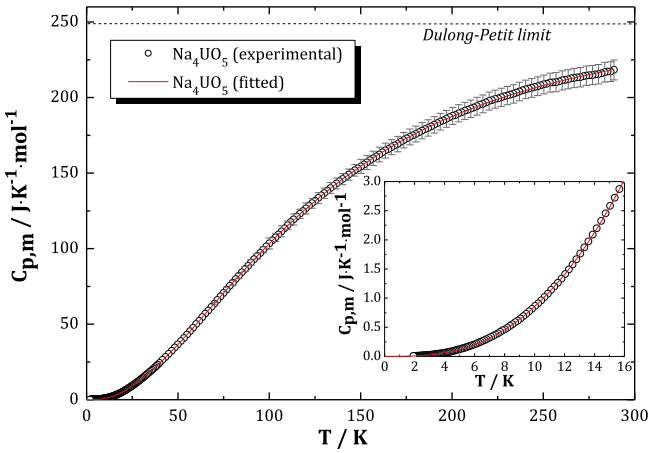

FIGURE 1. Heat capacity of Na_4UO_5 (○) and fit to the data (red line) as a function of temperature over the temperature range (1.9 to 288.7) K. The inset shows the data below $T = 16$ K. (For interpretation of the references to color in this figure legend, the reader is referred to the web version of this article.)

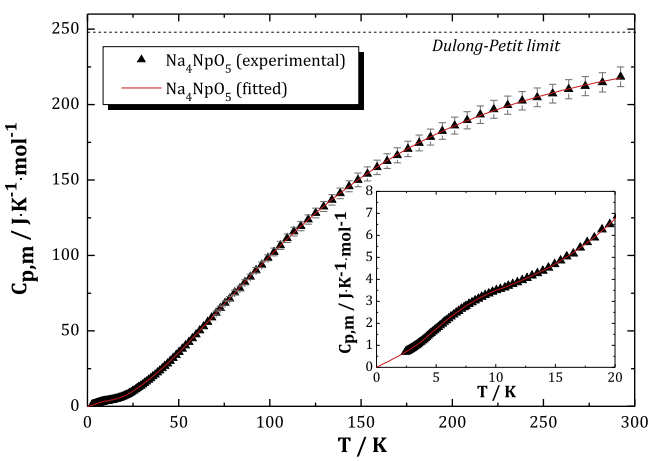

FIGURE 2. Heat capacity of Na_4NpO_5 (▲) and fit to the data (red line) as a function of temperature over the temperature range (2.4 to 292.2) K. The inset shows the data below $T = 20$ K. (For interpretation of the references to color in this figure legend, the reader is referred to the web version of this article.)

TABLE 1
Provenance and purity of the samples used in this study.

Formula	Source	State	Color	Mass fraction purity
Na_2CO_3	Sigma	Powder	White	0.9995
NpO_2	ORNL	Powder	Black	>0.998
Na_4UO_5	NRG	Powder	Orange	0.984
Na_4NpO_5	Synthesized in-house	Powder	Lime green	0.995

4. Discussion

The heat capacity at constant volume, $C_{V,m}$, is given by the sum of the lattice vibrations, electronic, and magnetic contributions [31]. The relation between the heat capacity at constant pressure measured experimentally, $C_{p,m}$, and the heat capacity at constant volume, $C_{V,m}$, involves the isobaric thermal expansivity and isothermal compressibility of the material. At very low temperatures, the thermal expansivity is negligible, so that $C_{p,m} \approx C_{V,m}$.

TABLE 2
Summary of fitting parameters of the heat capacity of Na_4UO_5 and Na_4NpO_5 within the temperature ranges (20.0 to 288.7) K and (23.2 to 292.2) K, respectively.

Parameters	Na_4UO_5	Na_4NpO_5
n_D/mol	1.8158	1.3355
θ_D/K	170.64	141.97
n_{E1}/mol	4.3260	3.7476
θ_{E1}/K	301.48	270.70
n_{E2}/mol	4.1826	5.1818
θ_{E2}/K	579.00	542.98
$n_D + n_{E1} + n_{E2}$/mol	10.3244	10.2649
Temp. range/K	20.0–288.7	23.2–292.2
RMS%	31.1	29.6

TABLE 3
Summary of fitting parameters of the heat capacity of Na_4UO_5 and Na_4NpO_5 within the temperature ranges (1.9 to 20.0) K and (2.4 to 4.3) K, respectively.

Parameters	Na_4UO_5	Na_4NpO_5
δ/mJ · mol^{-1} · K^{-2}		274.59
B_3/mJ · mol^{-1} · K^{-4}	0.9897	1.5100
B_5/mJ · mol^{-1} · K^{-6}	$-1.7091 \cdot 10^{-3}$	$8.4578 \cdot 10^{-2}$
B_7/mJ · mol^{-1} · K^{-8}	$3.9306 \cdot 10^{-6}$	
B_9/mJ · mol^{-1} · K^{-10}	$-4.0657 \cdot 10^{-9}$	
Temp. range/K	1.9–20.0	2.4–4.3
RMS%	0.58	0.12

TABLE 4
Summary of fitting parameters used to model the broad Schottky-type anomaly observed in the heat capacity of Na_4NpO_5.

Parameters	Na_4NpO_5 (1)	Na_4NpO_5 (2)
B_3/mJ · mol^{-1} · K^{-4}	0.90728	0.90728
B_5/mJ · mol^{-1} · K^{-6}	$-7.0430 \cdot 10^{-4}$	$-7.0430 \cdot 10^{-4}$
B_7/mJ · mol^{-1} · K^{-8}	$2.7899 \cdot 10^{-7}$	$2.7899 \cdot 10^{-7}$
α_S	0.85	0.73
θ_S/K	20.1	22.9
ε_1/cm^{-1}	14.0	25.9

TABLE 5
Summary of thermodynamic data for Na_4UO_5 and Na_4NpO_5.

Phase	$\Delta_f H^o_m$(298.15 K) (kJ · mol^{-1})	S^o_m(298.15 K) (J · K^{-1} · mol^{-1})	$C^o_{p,m}$(298.15 K) (J · K^{-1} · mol^{-1})	$\Delta_f G^o_m$(298.15 K) (kJ · mol^{-1})
Na_4UO_5	-2457.0 ± 2.2 [15]	247.5 ± 6.2	220.6 ± 6.7	-2301.7 ± 2.9
Na_4NpO_5	-2315.4 ± 5.7 [15]	247.5 ± 6.2	219.0 ± 6.6	-2159.7 ± 6.0

4.1. Fitting of the lattice contribution above T = 20 K.

The lattice contribution dominates at temperatures above about $T = 20$ K, and can be modeled using a combination of Debye and Einstein functions, as written in Eq. (1). Two Einstein functions were needed in the present work to fit the data. Fitting with a single Einstein function was attempted, but could not reproduce accurately the high temperature region.

$$C_{p,m} = n_D D(\theta_D) + n_{E1} E(\theta_{E1}) + n_{E2} E(\theta_{E2}). \quad (1)$$

Here R is the universal gas constant equal to 8.3144621 J · K^{-1} · mol^{-1}, $D(\theta_D), E(\theta_{E1})$, and $E(\theta_{E2})$ are the Debye, low and high temperature Einstein functions, respectively, as written in Eqs. (2) and (3). θ_D, θ_{E1}, and θ_{E2} are the characteristic Debye and Einstein temperatures. n_D, n_{E1}, and n_{E2} are adjustable parameters, whose sum $(n_D + n_{E1} + n_{E2})$ should be approximately equal to the number of atoms in the formula unit (i.e., 10 in this case).

TABLE 6
Refined atomic positions in Na_4NpO_5. R_{wp} = 11.2%, R_{exp} = 4.53%, χ^2 = 6.1. 5578 points for pattern. 83 Refined parameters. Peak shape η: Pseudo-Voigt*Axial divergence asymmetry. Background: Linear interpolation between operator-selected points in the pattern.

Atom	Ox. State	Wyckoff	x	y	z	B_0 (Å^2)
Na	+1	8h	0.1970(5)	0.4035(5)	0	1.05(7)
Np	+6	2a	0	0	0	0.51(1)
O1	−2	2b	0	0	0.5	1.67(10)
O2	−2	8h	0.264(1)	0.082(1)	0	2.32(10)

TABLE 7
Selected bond lengths, R(Å), for Na_4NpO_5 derived from the X-ray diffraction data. Standard deviations are given in parentheses. N is the number of atoms in each coordination shell.

Bond	N	R (Å)
Np–O(1)	2	2.30(1)
Np–O(2)	4	2.09(1)
Na–O(1)	1	2.40(1)
Na–O(2)	2	2.32(1)
Na–O(2)	1	2.48(1)
Na–O(2)	1	2.36(1)
Na–O(2)	1	2.66(1)

$$D(\theta_D) = 9R\left(\frac{1}{x}\right)^3 \int_o^x \frac{\exp(x)x^4}{[\exp(x)-1]^2}\cdot \mathrm{dx}, \quad x = \frac{\theta_D}{T}, \tag{2}$$

$$E(\theta_E) = 3Rx^2 \frac{\exp(x)}{[\exp(x)-1]^2}, \quad x = \frac{\theta_E}{T}. \tag{3}$$

The fitted parameters obtained for Na_4UO_5 and Na_4Np_5 in the temperature regions (20.0 to 288.7) K and (23.2 to 292.2) K, respectively, are listed in table 4. The sum $(n_D + n_{E1} + n_{E2})$ is very close to 10. The Debye and Einstein temperatures are found systematically higher for the uranium compound, suggesting stronger bonding between the uranium cation and surrounding oxygen ions. The reverse behaviour would be expected, however, considering the respective bond lengths in the UO_6 [7] and NpO_6 octahedra [13], and ionic radii of the U^{6+} (0.73 Å) and Np^{6+} (0.72 Å) cations according to Shannon's tabulated data [32]. This result can be related to the fact that the experimental curves cross around T = 35 K, as seen in figure 3, and could be the effect of the 5f valence electrons since these compounds show different electronic configurations, namely $[Rn]5f^0$ for Na_4UO_5 and $[Rn]5f^1$ for Na_4NpO_5. An alternative explanation would be the interplay between force constant and atomic mass [33]. However, considering the uncertainty of the method, and especially of the encapsulation procedure in Stycast, it is not possible to definitively assign this feature to a physical phenomenon. Calculations of the phonon density of states and of the vibration modes would be required to conclude.

The root mean square deviation (RMS) of the fits are rather high, despite a good general agreement with the experimental data. Indeed, the deviation from the experimental results remains below 0.4% over the temperature range (20 to 292) K, as shown in figure 4. The RMS discrepancy can be related to the uncertainty on our experimental results, which increases towards high temperatures, mainly due to the correction for the Stycast contribution.

4.2. Fitting below T = 20 K.

At very low temperatures (T < 20 K), the phonon contribution is well-represented using an harmonic-lattice model [27], as expressed by Eq. (4), where the number of required terms augments with the high temperature limit of the fit:

$$C_{latt} = \sum B_n T^n, \quad \text{where} \quad n = 3, 5, 7, 9\ldots \tag{4}$$

The electronic contribution of the conduction electrons at the Fermi surface are represented with a linear term γT [34]. The electronic specific heat is zero for insulating materials such as Na_4UO_5 and Na_4NpO_5 (orange and lime green, respectively). However, recent studies have revealed that a linear term could nevertheless occur due to departure from stoichiometry, oxygen vacancies or defects within the material [27]. α-FeOOH [27], $Fe_2P_2O_7$ [35], and $Sr_2TiSi_2O_8$ [33] are example of such materials.

The heat capacity of Na_4UO_5 was fitted with the harmonic model using four terms to cover the rather large temperature range of the fit (1.9 to 20.0) K. The corresponding coefficients are listed in table 4. A simple two terms harmonic model was sufficient to cover the temperature range (2.4 to 4.3) K in the case of Na_4NpO_5. However, the addition of a linear δT term also appeared necessary to describe the experimental curve. The broad Schottly anomaly was fitted between T = (4.3 and 23.2) K using a series of cubic spline polynomials.

The need for a linear δT term to fit the Na_4NpO_5 data in the temperature range (2.4 to 4.3) K suggests the presence of a non negligible amount of oxygen vacancies or defects within the material [27]. This observation can be related to the particular peak profile shape observed in the X-ray diffraction pattern as detailed in Appendix A. The Bragg reflections indeed show an asymmetric profile in opposite directions for successive *hkl* reflections, which is particularly pronounced at low angles, as detailed in [13]. This feature was interpreted in our previous work as a slight heterogeneity within the material which creates stresses. In fact, the Rietveld refinement and the description of the peak profile shape can be improved by introducing a second tetragonal phase with slightly larger cell volume, which concurs with the hypothesis of the formation of oxygen vacancies or defects (see Appendix A). A departure from stoichiometry is unlikely, however, as the Mössbauer data showed no traces of pentavalent neptunium in this material [13]. Instead, it is suggested that oxygen Frenkel pairs might occur. The δT term is much larger than reported in the literature for this type of defects, however [27,33], which is rather puzzling. Self-heating effects coming from the radioactive decay of ^{237}Np were considered, but appeared negligible. The corresponding contribution amounts to no more than 0.5% at T = 2.5 K and 0.04% at T = 10 K of the signal. The physical interpretation of this phenomenon could therefore be more intricate.

4.3. Modelling the Schottky-type anomaly

The neptunium cation in Na_4NpO_5 is hexavalent, as confirmed by Mössbauer spectroscopy [13], and shows therefore a $[Rn]5f^1$ electronic configuration. The Np ion in this structure is therefore a Kramers ion with a $^2F_{5/2}$ ground state manifold and $^2F_{7/2}$ first excited state arising from spin–orbit coupling. The $^2F_{5/2}$ ground state has a degeneracy of $(2J+1) = 6$, and is subsequently split into three Kramers doublets (Γ_7 ground state, and Γ_7^t, Γ_6^t excited states) by the crystal field effect in the tetragonally distorted (D_{4h}) symmetry [13]. Our previous studies have shown that Na_4NpO_5 probably shows two low-lying states having the same degeneracy and separated by about 14 cm^{-1} [13]. It was therefore attempted in the present work to fit the anomaly in the heat capacity data using a simple two levels Schottky function as written in Eq. (5) [34]:

$$C_{Schottky} = R\left(\frac{\theta_S}{T}\right)^2 \frac{g_0}{g_1} \frac{\exp\left(\frac{\theta_S}{T}\right)}{\left(1+\frac{g_0}{g_1}\exp\left(\frac{\theta_S}{T}\right)\right)^2}, \tag{5}$$

TABLE 8
Experimental heat capacity data[a] for Na_4UO_5 measured at pressure p = 1.233 mPa[b]. The reported data were corrected for 1.6 wt% α-Na_2UO_4 impurity [25]. R is the ideal gas constant equal to 8.3144621 $J \cdot K^{-1} \cdot mol^{-1}$.

T/K	$C^o_{p,m}$/$J \cdot K^{-1} \cdot mol^{-1}$	$C^o_{p,m}/R$	T/K	$C^o_{p,m}$/$J \cdot K^{-1} \cdot mol^{-1}$	$C^o_{p,m}/R$	T/K	$C^o_{p,m}$/$J \cdot K^{-1} \cdot mol^{-1}$	$C^o_{p,m}/R$	T/K	$C^o_{p,m}$/$J \cdot K^{-1} \cdot mol^{-1}$	$C^o_{p,m}/R$
1.92	0.00593	$7.1322 \cdot 10^{-4}$	8.71	0.588	0.0707	39.95	24.347	2.928	165.25	165.91	19.95
1.95	0.00639	$7.6854 \cdot 10^{-4}$	8.89	0.615	0.0739	41.62	26.309	3.164	166.92	167.14	20.10
1.99	0.00660	$7.9380 \cdot 10^{-4}$	9.07	0.651	0.0783	43.29	28.298	3.403	168.59	168.30	20.24
2.03	0.00709	$8.5273 \cdot 10^{-4}$	9.26	0.691	0.0831	44.96	30.351	3.650	170.26	169.22	20.35
2.07	0.00747	$8.9844 \cdot 10^{-4}$	9.45	0.728	0.0876	46.63	32.399	3.897	171.93	170.63	20.52
2.11	0.00821	$9.8744 \cdot 10^{-4}$	9.64	0.771	0.0928	48.30	34.486	4.148	173.60	171.73	20.65
2.16	0.00865	$1.040 \cdot 10^{-3}$	9.84	0.816	0.0981	49.96	36.580	4.400	175.27	172.85	20.79
2.20	0.00919	$1.110 \cdot 10^{-3}$	10.04	0.864	0.1039	51.64	38.704	4.655	176.94	173.92	20.92
2.25	0.00977	$1.180 \cdot 10^{-3}$	10.25	0.908	0.1092	53.30	40.820	4.910	178.61	175.00	21.05
2.29	0.0102	$1.230 \cdot 10^{-3}$	10.46	0.962	0.1157	54.98	43.053	5.178	180.28	175.82	21.15
2.34	0.0113	$1.360 \cdot 10^{-3}$	10.67	1.0161	0.1222	56.64	45.303	5.449	181.95	177.05	21.29
2.38	0.0117	$1.400 \cdot 10^{-3}$	10.89	1.0725	0.1290	58.32	47.545	5.718	183.61	178.04	21.41
2.43	0.0128	$1.540 \cdot 10^{-3}$	11.11	1.1392	0.1370	59.99	49.956	6.008	185.28	179.00	21.53
2.48	0.0134	$1.610 \cdot 10^{-3}$	11.34	1.1998	0.1443	61.67	52.216	6.280	186.95	179.87	21.63
2.53	0.0143	$1.720 \cdot 10^{-3}$	11.57	1.2632	0.1519	63.33	54.606	6.568	188.62	180.89	21.76
2.58	0.0154	$1.850 \cdot 10^{-3}$	11.81	1.3339	0.1604	64.99	56.902	6.844	190.30	181.94	21.88
2.63	0.0161	$1.940 \cdot 10^{-3}$	12.05	1.4125	0.1699	66.67	58.963	7.092	191.96	183.02	22.01
2.69	0.0175	$2.100 \cdot 10^{-3}$	12.30	1.4924	0.1795	68.34	61.380	7.382	193.63	184.02	22.13
2.74	0.0186	$2.240 \cdot 10^{-3}$	12.55	1.5738	0.1893	70.00	63.597	7.649	195.32	184.77	22.22
2.80	0.0203	$2.440 \cdot 10^{-3}$	12.81	1.6681	0.2006	71.67	65.956	7.933	196.97	185.87	22.35
2.85	0.0206	$2.480 \cdot 10^{-3}$	13.06	1.7629	0.2120	73.35	68.269	8.211	198.64	186.91	22.48
2.91	0.0212	$2.550 \cdot 10^{-3}$	13.33	1.8701	0.2249	75.01	70.592	8.490	200.31	187.85	22.59
2.97	0.0247	$2.960 \cdot 10^{-3}$	13.60	1.9728	0.2373	76.69	72.935	8.772	201.98	188.42	22.66
3.03	0.0260	$3.130 \cdot 10^{-3}$	13.88	2.0882	0.2512	78.36	75.296	9.056	203.65	189.55	22.80
3.09	0.0270	$3.240 \cdot 10^{-3}$	14.16	2.1993	0.2645	80.04	77.375	9.306	205.31	190.19	22.87
3.16	0.0293	$3.520 \cdot 10^{-3}$	14.45	2.3245	0.2796	81.71	79.782	9.596	206.98	191.15	22.99
3.22	0.0313	$3.760 \cdot 10^{-3}$	14.74	2.4536	0.2951	83.38	82.033	9.866	208.64	191.78	23.07
3.28	0.0325	$3.910 \cdot 10^{-3}$	15.04	2.5813	0.3105	85.04	84.258	10.13	210.32	192.62	23.17
3.35	0.0335	$4.020 \cdot 10^{-3}$	15.35	2.7223	0.3274	86.72	86.463	10.40	211.99	193.38	23.26
3.42	0.0372	$4.470 \cdot 10^{-3}$	15.66	2.8701	0.3452	88.39	88.563	10.65	213.66	194.27	23.36
3.49	0.0399	$4.800 \cdot 10^{-3}$	15.98	3.0319	0.3647	90.05	90.767	10.92	215.32	195.25	23.48
3.56	0.0424	$5.100 \cdot 10^{-3}$	16.32	3.2008	0.3850	91.72	92.988	11.18	216.99	195.84	23.55
3.63	0.0451	$5.430 \cdot 10^{-3}$	16.63	3.3660	0.4048	93.38	95.047	11.43	218.66	196.75	23.66
3.71	0.0473	$5.690 \cdot 10^{-3}$	17.00	3.5489	0.4268	95.06	97.096	11.68	220.32	197.67	23.77
3.78	0.0522	$6.270 \cdot 10^{-3}$	17.34	3.7540	0.4515	96.73	99.204	11.93	221.98	198.23	23.84
3.86	0.0536	$6.440 \cdot 10^{-3}$	17.70	3.9711	0.4776	98.39	101.40	12.20	223.65	198.97	23.93
3.94	0.0578	$6.960 \cdot 10^{-3}$	18.06	4.1908	0.5040	100.07	103.46	12.44	225.31	199.42	23.99
4.03	0.0613	$7.370 \cdot 10^{-3}$	18.42	4.4038	0.5297	101.74	105.45	12.68	226.98	200.17	24.08
4.10	0.0667	$8.020 \cdot 10^{-3}$	18.80	4.6251	0.5563	103.40	107.42	12.92	228.64	200.83	24.15
4.19	0.0694	$8.340 \cdot 10^{-3}$	19.17	4.8500	0.5833	105.08	109.35	13.15	230.30	201.33	24.21
4.28	0.0745	$8.960 \cdot 10^{-3}$	19.57	5.0977	0.6131	106.75	111.42	13.40	231.97	201.90	24.28
4.36	0.0811	$9.750 \cdot 10^{-3}$	19.98	5.4070	0.6503	108.40	113.42	13.64	233.64	202.39	24.34
4.45	0.0844	0.0101	20.37	5.6465	0.6791	110.08	115.46	13.89	235.32	203.19	24.44
4.54	0.0900	0.0108	20.80	5.9563	0.7164	111.76	117.47	14.13	236.98	203.97	24.53
4.64	0.0959	0.0115	21.21	6.2423	0.7508	113.43	119.30	14.35	238.65	204.81	24.63
4.73	0.103	0.0124	21.65	6.5652	0.7896	115.11	121.22	14.58	240.31	205.37	24.70
4.83	0.109	0.0132	22.09	6.8973	0.8296	116.77	123.02	14.80	241.98	205.95	24.77
4.93	0.115	0.0139	22.54	7.2516	0.8722	118.45	124.84	15.01	243.65	206.36	24.82
5.03	0.123	0.0148	23.00	7.6106	0.9153	120.11	126.59	15.23	245.31	206.87	24.88
5.13	0.131	0.0158	23.49	7.9300	0.9538	121.79	128.34	15.44	246.97	207.46	24.95
5.24	0.140	0.0168	23.95	8.3169	1.000	123.45	130.03	15.64	248.64	208.04	25.02
5.34	0.146	0.0176	24.47	8.7734	1.055	125.13	131.61	15.83	250.30	208.66	25.10
5.45	0.158	0.0190	24.93	9.1949	1.106	126.79	133.50	16.06	251.97	209.12	25.15
5.56	0.166	0.0200	25.47	9.6060	1.155	128.48	135.13	16.25	253.63	209.84	25.24
5.68	0.176	0.0211	25.99	10.053	1.209	130.15	136.65	16.44	255.29	209.94	25.25
5.79	0.186	0.0224	26.50	10.509	1.264	131.82	138.32	16.64	256.95	210.17	25.28
5.91	0.196	0.0236	27.05	10.997	1.323	133.49	140.08	16.85	258.61	210.66	25.34
6.03	0.210	0.0252	27.60	11.494	1.382	135.16	141.63	17.03	260.28	211.34	25.42
6.16	0.222	0.0267	28.16	12.018	1.445	136.83	143.06	17.21	261.94	211.66	25.46
6.28	0.234	0.0282	28.74	12.564	1.511	138.50	144.61	17.39	263.60	212.09	25.51
6.41	0.249	0.0299	29.33	13.129	1.579	140.18	146.03	17.56	265.27	212.68	25.58
6.54	0.264	0.0317	29.92	13.703	1.648	141.84	147.42	17.73	266.94	212.89	25.60
6.68	0.279	0.0335	30.53	14.287	1.718	143.51	149.03	17.92	268.60	213.30	25.65
6.81	0.295	0.0355	31.16	14.896	1.792	145.18	150.44	18.09	270.26	213.48	25.68
6.96	0.315	0.0379	31.79	15.543	1.869	146.86	151.79	18.26	271.93	214.09	25.75
7.12	0.333	0.0401	32.44	16.180	1.946	148.52	153.11	18.42	273.59	214.46	25.79
7.27	0.355	0.0427	33.10	16.863	2.028	150.20	154.41	18.57	275.25	214.75	25.83
7.41	0.375	0.0451	33.78	17.567	2.113	151.87	155.67	18.72	276.92	214.85	25.84
7.57	0.395	0.0475	34.49	18.263	2.197	153.54	157.06	18.89	278.58	215.27	25.89
7.72	0.420	0.0506	35.20	19.006	2.286	155.21	158.47	19.06	280.24	215.47	25.92
7.88	0.447	0.0538	35.91	19.759	2.376	156.89	159.73	19.21	281.90	215.98	25.98

(*continued on next page*)

TABLE 8 (*continued*)

T/K	$C^o_{p,m}$/J · K^{-1} · mol^{-1}	$C^o_{p,m}/R$	T/K	$C^o_{p,m}$/J · K^{-1} · mol^{-1}	$C^o_{p,m}/R$	T/K	$C^o_{p,m}$/J · K^{-1} · mol^{-1}	$C^o_{p,m}/R$	T/K	$C^o_{p,m}$/J · K^{-1} · mol^{-1}	$C^o_{p,m}/R$
8.04	0.465	0.0560	36.64	20.564	2.473	158.57	161.07	19.37	283.56	216.80	26.07
8.20	0.492	0.0592	37.40	21.409	2.575	160.24	162.31	19.52	285.22	217.10	26.11
8.37	0.524	0.0630	38.16	22.257	2.677	161.90	163.70	19.69	286.87	217.15	26.12
8.54	0.551	0.0663	38.93	23.126	2.781	163.57	164.92	19.84	288.66	218.27	26.25

[a] The standard uncertainties u on the temperature are: $u(T)$ = 0.01 K for 1.9 < T/K < 20, $u(T)$ = 0.02 K for 20 < T/K < 100, $u(T)$ = 0.05 K for 100 < T/K < 300. The combined relative standard uncertainties on the values of the heat capacities are determined to be $u_r(C_{p,m})$ = 0.03 for T/K < 10, $u_r(C_{p,m})$ = 0.01 for 10 < T/K < 70, $u_r(C_{p,m})$ = 0.02 for 70 < T/K < 100, $u_r(C_{p,m})$ = 0.025 for 100 < T/K < 150, and $u_r(C_{p,m})$ = 0.03 for T/K > 150.
[b] The standard uncertainty u on the pressure is: $u(p)$ = 0.009 mPa.

where θ_S is the spacing between the two low-lying electronic levels expressed in K, g_0 and g_1 their respective degeneracy ($g_0/g_1 = 1$ in this case). θ_S is related to the energy separation ε_1 between the two levels via the formula $\theta_S = \varepsilon_1/k_B$, where k_B is Boltzmann constant equal to $1.3806488 \cdot 10^{-23}$ J · K^{-1}.

The heat capacity of Na_4NpO_5 was thereafter represented using the aforementioned function together with a three terms harmonic model as written in Eq. (6). The corresponding coefficients are listed in table 4.

$$C_{p,m}(Na_4NpO_5, cr, T) = B_3T^3 + B_5T^5 + B_7T^7 + \alpha_S C_{Schottky}, \quad (6)$$

where α_S is a scaling factor adjusting the amplitude of the theoretical Schottky function to the one actually observed in the experiment.

The maximum temperature of the broad anomaly is fairly well described with such model as shown in figure 5. The spacing between the two low-lying electronic levels is at about T = (20.1 to 22.9) K, which corresponds to an energy separation of (14 to 15.9) cm^{-1}, in good agreement with our previous study [13]. The combination of the simple two levels Schottky function and harmonic model is not sufficient, however, to describe adequately both the width and intensity of the data below T = 6.5 K. The experimental ($C_{p,m}/T$) curve saturates at about 275 J · K^{-2} · mol^{-1}

TABLE 9
Experimental heat capacity data[a] for Na_4NpO_5 measured at pressure p = 1.233 mPa[b]. The reported data were corrected for 0.5 wt% α-Na_2NpO_4 impurity [26]. R is the ideal gas constant equal to 8.3144621 J · K^{-1} · mol^{-1}.

T/K	$C^o_{p,m}$/J · K^{-1} · mol^{-1}	$C^o_{p,m}/R$	T/K	$C^o_{p,m}$/J · K^{-1} · mol^{-1}	$C^o_{p,m}/R$	T/K	$C^o_{p,m}$/J · K^{-1} · mol^{-1}	$C^o_{p,m}/R$	T/K	$C^o_{p,m}$/J · K^{-1} · mol^{-1}	$C^o_{p,m}/R$
2.45	0.70490	0.08478	7.12	2.6612	0.3201	24.77	9.9987	1.203	89.31	85.845	10.32
2.50	0.71848	0.08641	7.35	2.7249	0.3277	25.60	10.525	1.266	92.43	90.203	10.85
2.55	0.73698	0.08864	7.51	2.7831	0.3347	26.51	11.225	1.350	95.57	93.800	11.28
2.61	0.75366	0.09064	7.75	2.8785	0.3462	27.34	11.963	1.439	98.91	98.385	11.83
2.67	0.77466	0.09317	8.01	2.9485	0.3546	28.28	12.767	1.536	102.30	102.34	12.31
2.73	0.79286	0.09536	8.27	3.0341	0.3649	29.25	13.606	1.636	105.76	106.62	12.82
2.80	0.81229	0.09770	8.54	3.1179	0.3750	30.25	14.511	1.745	109.46	111.36	13.39
2.87	0.83549	0.1005	8.82	3.2051	0.3855	31.29	15.443	1.857	113.18	115.85	13.93
2.94	0.86034	0.1035	9.11	3.2834	0.3949	32.38	16.421	1.975	116.98	119.41	14.36
3.01	0.88756	0.1068	9.42	3.3551	0.4035	33.50	17.463	2.100	121.02	123.80	14.89
3.09	0.91791	0.1104	9.73	3.4302	0.4126	34.65	18.594	2.236	125.19	128.19	15.42
3.17	0.94721	0.1139	10.05	3.4996	0.4209	35.85	19.774	2.378	129.51	132.43	15.93
3.26	0.97847	0.1177	10.39	3.5645	0.4287	37.08	21.005	2.526	133.99	136.86	16.46
3.35	1.0102	0.1215	10.75	3.6224	0.4357	38.35	22.319	2.684	138.61	141.15	16.98
3.44	1.0462	0.1258	11.06	3.6978	0.4447	39.67	23.667	2.846	143.40	145.80	17.54
3.54	1.0850	0.1305	11.43	3.7817	0.4548	41.03	25.150	3.025	148.36	150.07	18.05
3.64	1.1295	0.1358	11.82	3.8630	0.4646	42.44	26.686	3.210	153.46	154.06	18.53
3.74	1.1692	0.1406	12.21	3.9576	0.4760	43.89	28.328	3.407	158.77	158.40	19.05
3.85	1.2177	0.1465	12.62	4.0521	0.4874	45.36	30.051	3.614	164.23	162.51	19.55
3.96	1.2634	0.1520	13.05	4.1628	0.5007	47.01	31.939	3.841	169.89	166.34	20.01
4.08	1.3175	0.1585	13.50	4.2716	0.5138	48.62	33.994	4.089	175.75	170.60	20.52
4.20	1.3760	0.1655	13.95	4.3849	0.5274	50.28	35.980	4.327	181.80	174.59	21.00
4.32	1.4347	0.1726	14.42	4.5254	0.5443	52.03	38.140	4.587	188.06	178.47	21.47
4.45	1.4997	0.1804	14.93	4.6819	0.5631	53.78	40.320	4.849	194.56	182.52	21.95
4.58	1.5616	0.1878	15.43	4.8503	0.5834	55.66	42.651	5.130	201.26	186.09	22.38
4.72	1.6229	0.1952	15.96	5.0366	0.6058	57.57	45.008	5.413	208.19	189.61	22.80
4.87	1.6834	0.2025	16.50	5.1695	0.6218	59.53	47.601	5.725	215.38	193.34	23.25
5.02	1.7530	0.2108	17.09	5.4416	0.6545	61.59	50.208	6.039	222.76	196.86	23.68
5.18	1.8274	0.2198	17.66	5.6846	0.6837	63.70	52.949	6.368	230.42	199.63	24.01
5.34	1.8994	0.2285	18.27	5.8974	0.7093	65.88	55.908	6.724	238.37	202.54	24.36
5.51	1.9794	0.2381	18.91	6.2590	0.7528	68.16	58.818	7.074	246.59	204.81	24.63
5.68	2.0660	0.2485	19.56	6.4976	0.7815	70.52	61.879	7.442	255.08	207.29	24.93
5.87	2.1356	0.2569	20.23	6.8914	0.8288	72.93	65.058	7.825	263.86	210.20	25.28
6.05	2.2158	0.2665	20.92	7.2645	0.8737	75.44	68.365	8.222	272.95	212.24	25.53
6.25	2.3078	0.2776	21.65	7.6765	0.9233	78.00	71.370	8.584	282.35	214.72	25.83
6.46	2.3937	0.2879	22.39	8.1704	0.9827	80.70	75.402	9.069	292.25	218.40	26.27
6.68	2.4782	0.2981	23.16	8.6915	1.045	83.52	78.164	9.401			
6.89	2.5563	0.3075	23.97	9.2049	1.107	86.34	82.246	9.892			

[a] The standard uncertainties u on the temperature are: $u(T)$ = 0.01 K for 1.9 < T/K < 20, $u(T)$ = 0.02 K for 20 < T/K < 100, $u(T)$=0.05 K for 100 < T/K < 300. The combined relative standard uncertainties on the values of the heat capacities are determined to be $u_r(C_{p,m})$ = 0.03 for T/K < 10, $u_r(C_{p,m})$ = 0.01 for 10 < T/K < 70, $u_r(C_{p,m})$ = 0.02 for 70 < T/K < 100, $u_r(C_{p,m})$ = 0.025 for 100 < T/K < 150, and $u_r(C_{p,m})$ = 0.03 for T/K > 150.
[b] The standard uncertainty u on the pressure is: $u(p)$ = 0.009 mPa.

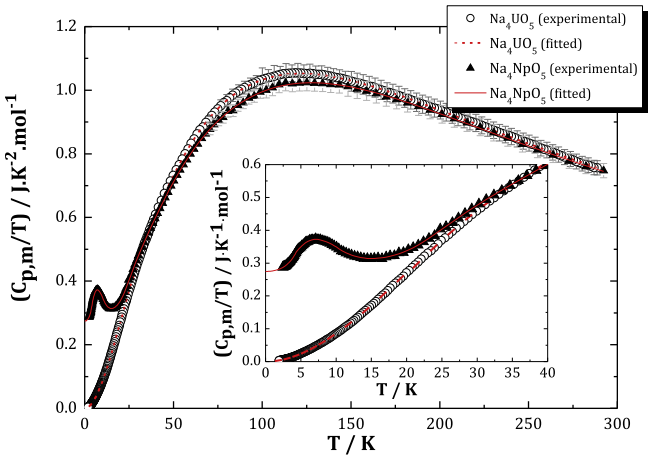

FIGURE 3. $C_{p,m}/T$ for Na_4UO_5 (○) and Na_4NpO_5(▲) measured in zero magnetic field, and fit to the data (plain and dotted lines).

instead of going to zero when reaching $T = 0$ K, probably due to the presence of defects within the material as detailed previously. This effect makes it more difficult to describe the anomaly with a theoretical Schottky function. Moreover, the associated entropy is less ($\alpha_{S1} = 0.85,\ \alpha_{S2} = 0.73$) than predicted by theory ($\Delta S_{Schottky} = R\ln 2 = 5.76\ \mathrm{J \cdot K^{-1} \cdot mol^{-1}}$), which also renders the fitting procedure more intricate. We have therefore preferred in the present work to fit the broad Schottky anomaly with a series of cubic spline polynomials so as to derive the thermodynamic functions between $T = (0$ and $300)$ K.

4.4. Derivation of thermodynamic functions

The empirical Neumann–Kopp (NK) rule, which suggests that the heat capacity of a solid is the sum of the heat capacity of its constituent chemical components, is usually a good approximation for the estimation of the specific heat at $T = 298.15$ K [36]. From the data of UO_3 [37] and Na_2O [38], the heat capacity of Na_4UO_5 can be estimated as $219.9\ \mathrm{J \cdot K^{-1} \cdot mol^{-1}}$, in very good agreement with our

TABLE 10
Standard thermodynamic functions for Na_4UO_5 at pressure $p = 100$ kPa. $\phi^o_m(T) = S^o_m(T) - [H^o_m(T) - H^o_m(0)]/T$.[a]

T/K	$C^o_{p,m}/(\mathrm{J \cdot K^{-1} \cdot mol^{-1}})$	$S^o_m/(\mathrm{J \cdot K^{-1} \cdot mol^{-1}})$	$H^o_m(T) - H^o_m(0)/(\mathrm{kJ \cdot mol^{-1}})$	$\phi^o_m(T)/(\mathrm{J \cdot K^{-1} \cdot mol^{-1}})$
0	0	0	0	
1	$9.8800 \cdot 10^{-4}$	$3.3120 \cdot 10^{-4}$	$2.4961 \cdot 10^{-7}$	$8.1595 \cdot 10^{-5}$
2	$7.8600 \cdot 10^{-3}$	$2.7900 \cdot 10^{-3}$	$4.6753 \cdot 10^{-6}$	$4.5340 \cdot 10^{-4}$
3	0.026320	$9.1400 \cdot 10^{-3}$	$2.1765 \cdot 10^{-5}$	$1.8900 \cdot 10^{-3}$
4	0.061650	0.021240	$6.5749 \cdot 10^{-5}$	$4.8000 \cdot 10^{-3}$
5	0.11867	0.040810	$1.5591 \cdot 10^{-4}$	$9.6300 \cdot 10^{-3}$
6	0.20154	0.069470	$3.1602 \cdot 10^{-4}$	0.016800
7	0.31382	0.10868	$5.7370 \cdot 10^{-4}$	0.026730
8	0.45842	0.15975	$9.5982 \cdot 10^{-4}$	0.039770
9	0.63780	0.22383	$1.5100 \cdot 10^{-3}$	0.056290
10	0.85403	0.30197	$2.2500 \cdot 10^{-3}$	0.076580
11	1.1091	0.39508	$3.2400 \cdot 10^{-3}$	0.10096
12	1.4048	0.50402	$4.4900 \cdot 10^{-3}$	0.12967
13	1.7433	0.62961	$6.0700 \cdot 10^{-3}$	0.16297
14	2.1269	0.77262	$8.0000 \cdot 10^{-3}$	0.20109
15	2.5577	0.93383	0.010340	0.24425
16	3.0374	1.1140	0.013140	0.29268
17	3.5665	1.3138	0.016440	0.34658
18	4.1424	1.5338	0.020300	0.40614
19	4.7580	1.7741	0.024750	0.47155
20	5.3980	2.0342	0.029830	0.54293
25	9.2442	3.6289	0.065940	0.99148
30	13.806	5.7097	0.12336	1.5977
35	18.832	8.2093	0.20477	2.3586
40	24.311	11.076	0.31245	3.2653
45	30.237	14.278	0.44865	4.3078
50	36.554	17.787	0.61548	5.4776
55	43.165	21.579	0.81468	6.7668
60	49.967	25.626	1.0475	8.1680
65	56.865	29.897	1.3145	9.6737
70	63.783	34.364	1.6161	11.277
75	70.662	39.000	1.9523	12.969
80	77.460	43.778	2.3226	14.745
85	84.144	48.675	2.7267	16.596
90	90.688	53.670	3.1638	18.517
95	97.076	58.745	3.6333	20.500
100	103.29	63.883	4.1343	22.540
110	115.16	74.291	5.2272	26.771
120	126.23	84.791	6.4348	31.168
130	136.48	95.305	7.7490	35.697
140	145.91	105.77	9.1617	40.329
150	154.55	116.14	10.665	45.038
160	162.44	126.37	12.250	49.802
170	169.62	136.43	13.911	54.603
180	176.14	146.32	15.640	59.425
190	182.08	156.00	17.432	64.254
200	187.46	165.48	19.280	69.079
210	192.36	174.75	21.180	73.891

(*continued on next page*)

TABLE 10 (*continued*)

T/K	$C^{o}_{p,m}$/(J · K^{-1} · mol^{-1})	S^{o}_{m}/(J · K^{-1} · mol^{-1})	$H^{o}_{m}(T) - H^{o}_{m}(0)$/(kJ · mol^{-1})	$\phi^{o}_{m}(T)$/(J · K^{-1} · mol^{-1})
220	196.82	183.80	23.126	78.682
230	200.87	192.64	25.115	83.445
240	204.57	201.27	27.142	88.175
250	207.95	209.69	29.205	92.868
260	211.03	217.90	31.300	97.520
270	213.86	225.92	33.425	102.13
273.15	214.70	228.41	34.100	103.57
280	216.45	233.75	35.576	106.69
290	218.83	241.39	37.753	111.20
298.15	220.63	247.48	39.544	114.84
300	221.02	248.84	39.952	115.67

[a] The relative combined standard uncertainties in the values of the fitted heat capacities are determined from the experimental and fitted uncertainties to be $u_r(\mathrm{Cp,m}) = 0.031$ for $T/\mathrm{K} < 10$, $u_r(\mathrm{Cp,m}) = 0.011$ for $10 < T/\mathrm{K} < 70$, $u_r(\mathrm{Cp,m}) = 0.021$ for $70 < T/\mathrm{K} < 100$, $u_r(\mathrm{Cp,m}) = 0.026$ for $100 < T/\mathrm{K} < 150$, and $u_r(\mathrm{Cp,m}) = 0.031$ for $T/\mathrm{K} > 150$. The standard uncertainty on the pressure is $u(p) = 5$ kPa.

TABLE 11
Standard thermodynamic functions for Na_4NpO_5 at pressure $p = 100$ kPa. $\phi^{o}_{m}(T) = S^{o}_{m}(T) - [H^{o}_{m}(T) - H^{o}_{m}(0)]/T$.[a]

T/K	$C^{o}_{p,m}$/(J · K^{-1} · mol^{-1})	S^{o}_{m}/(J · K^{-1} · mol^{-1})	$H^{o}_{m}(T) - H^{o}_{m}(0)$/(kJ · mol^{-1})	$\phi^{o}_{m}(T)$/(J · K^{-1} · mol^{-1})
0	0	0	0	
0.5	0.13749	0.12363	$3.4349 \cdot 10^{-5}$	0.054930
1	0.27618	0.26138	$1.3769 \cdot 10^{-4}$	0.12369
2	0.56397	0.54047	$5.5777 \cdot 10^{-4}$	0.26158
3	0.88509	0.82897	$1.2800 \cdot 10^{-3}$	0.40154
4	1.2816	1.1367	$2.3700 \cdot 10^{-3}$	0.54528
4.5	1.5181	1.3013	$3.0700 \cdot 10^{-3}$	0.62004
5	1.7469	1.4730	$3.8800 \cdot 10^{-3}$	0.69661
5.5	1.9739	1.6501	$4.8100 \cdot 10^{-3}$	0.77513
6	2.1955	1.8313	$5.8500 \cdot 10^{-3}$	0.85552
7	2.6069	2.2005	$8.2600 \cdot 10^{-3}$	1.0211
8	2.9537	2.5713	0.011040	1.1918
9	3.2520	2.9365	0.014140	1.3656
10	3.4939	3.2919	0.017510	1.5407
11	3.6937	3.6345	0.021110	1.7158
12	3.9126	3.9654	0.024910	1.8897
13	4.1508	4.2881	0.028940	2.0619
14	4.4035	4.6050	0.033220	2.2323
15	4.7077	4.9192	0.037770	2.4010
16	5.0394	5.2336	0.042650	2.5682
17	5.4041	5.5500	0.047870	2.7342
18	5.8071	5.8703	0.053470	2.8995
19	6.2539	6.1962	0.059500	3.0643
20	6.7498	6.5295	0.066010	3.2292
25	10.055	8.3652	0.10745	4.0670
30	14.294	10.568	0.16819	4.9614
35	18.933	13.113	0.25107	5.9399
40	24.048	15.970	0.35833	7.0118
45	29.625	19.120	0.49234	8.1793
50	35.575	22.547	0.65522	9.4423
55	41.791	26.227	0.84855	10.799
60	48.177	30.136	1.0734	12.246
65	54.660	34.248	1.3305	13.779
70	61.189	38.537	1.6201	15.393
75	67.724	42.982	1.9424	17.083
80	74.236	47.561	2.2973	18.844
85	80.695	52.255	2.6847	20.671
90	87.078	57.049	3.1041	22.558
95	93.361	61.925	3.5553	24.502
100	99.522	66.871	4.0375	26.496
110	111.40	76.919	5.0927	30.622
120	122.60	87.098	6.2633	34.904
130	133.03	97.328	7.5421	39.312
140	142.68	107.54	8.9213	43.821
150	151.52	117.69	10.393	48.408
160	159.61	127.74	11.949	53.053
170	166.97	137.64	13.583	57.738
180	173.66	147.37	15.286	62.448
190	179.74	156.93	17.054	67.170
200	185.25	166.29	18.879	71.893
210	190.26	175.45	20.757	76.607

TABLE 11 (*continued*)

T/K	$C^o_{p,m}$/(J · K^{-1} · mol^{-1})	S^o_m/(J · K^{-1} · mol^{-1})	$H^o_m(T) - H^o_m(0)$/(kJ · mol^{-1})	$\phi^o_m(T)$/(J · K^{-1} · mol^{-1})
220	194.81	184.41	22.683	81.304
230	198.94	193.16	24.652	85.978
240	202.71	201.71	26.661	90.623
250	206.14	210.05	28.705	95.234
260	209.28	218.20	30.782	99.807
270	212.15	226.15	32.890	104.34
273.15	213.00	228.62	33.559	105.76
280	214.77	233.92	35.025	108.83
290	217.18	241.50	37.185	113.27
298.15	219.01	247.54	38.962	116.86
300	219.40	248.90	39.368	117.67

[a] The combined standard uncertainties in the values of the fitted heat capacities are determined from the experimental and fitted uncertainties to be $u_r(C_{p,m})$ = 0.03 for T/K < 10, $u_r(C_{p,m})$ = 0.011 for 10 < T/K < 70, $u_r(C_{p,m})$ = 0.02 for 70 < T/K < 100, $u_r(C_{p,m})$ = 0.025 for 100 < T/K < 150, and $u_r(C_{p,m})$ = 0.03 for T/K > 150. The standard uncertainty on the pressure is $u(p)$ = 5 kPa.

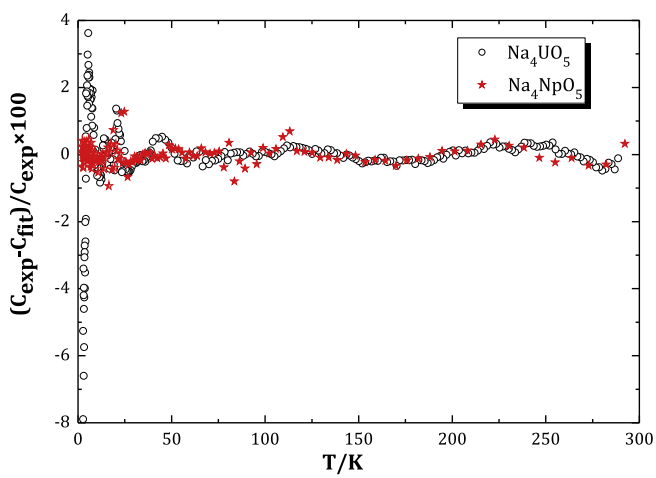

FIGURE 4. Deviation of the fitting equations from the experimental data for Na_4UO_5 (○) and Na_4NpO_5 (★).

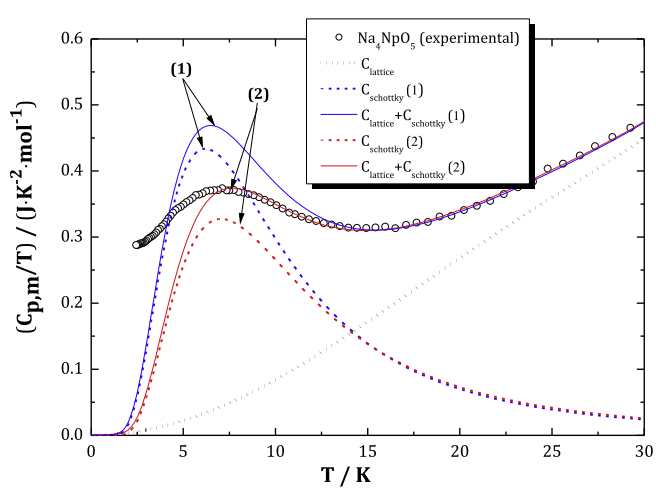

FIGURE 5. $C_{p,m}/T$ for Na_4NpO_5 (○) measured in zero magnetic field below T = 30 K, and fitting using a combination of a Schottky function (dotted line) and harmonic lattice contribution (short dotted line). The configuration (1) corresponds to $\varepsilon_1 = 14\ \mathrm{cm}^{-1}$ and $\alpha_S = 0.85$. The configuration (2) corresponds to $\varepsilon_1 = 15.9\ \mathrm{cm}^{-1}$ and $\alpha_S = 0.73$.

experimental results. The sum of the heat capacities of NpO_2 [37], Na_2O [38], and Na_2O_2 [38] gives 224.6 J · K^{-1} · mol^{-1} for Na_4NpO_5. The comparison is not ideal, however, as the neptunium adopts different oxidation states in Na_4NpO_5 and NpO_2, namely (VI) and (IV), respectively. The local structural environment around the neptunium cation is also different (6-fold coordination in Na_4NpO_5, but 8-fold coordination in NpO_2). A more appropriate comparison is with the sum of α-Na_2NpO_4 [26] and Na_2O [38], which amounts to 221.0 J · K^{-1} · mol^{-1}, in very good agreement with the experiment.

Combining our newly determined values of the standard entropies with the ones for sodium [39,15], uranium [37], neptunium [37], and oxygen [39], the standard entropies of formation of Na_4UO_5 and Na_4NpO_5 were estimated as $\Delta_f S^o_m(Na_4UO_5, cr, 298.15\ K) = -(520.8 \pm 6.3)\ J \cdot K^{-1} \cdot mol^{-1}$ and $\Delta_f S^o_m(Na_4NpO_5, cr, 298.15\ K) = -(521.0 \pm 6.3)\ J \cdot K^{-1} \cdot mol^{-1}$, respectively.

The enthalpies of formation reported for those compounds at T = 298.15 K [15] are listed in table 5. Using the aforementioned values for the standard entropies and enthalpies, the following standard Gibbs energies of formation were derived at T = 298.15 K: $\Delta_f G^o_m(Na_4UO_5, cr, 298.15\ K) = -(2301.7 \pm 2.9)\ kJ \cdot mol^{-1}$ and $\Delta_f G^o_m(Na_4NpO_5, cr, 298.15\ K) = -(2159.7 \pm 6.0)\ kJ \cdot mol^{-1}$, respectively.

Finally, considering the hypothetical dissociation reaction (7) for Na_4MO_5 (M = U, Np), the dissociation Gibbs energy is expressed by relation (8), where Na_4MO_5 and MO_2^{2+} have the same electronic state.

$$Na_4MO_5(cr) + 6H^+(aq) = 4\,Na^+(aq) + MO_2^{2+}(aq) + 3\,H_2O(l), \quad (7)$$

$$\begin{aligned}\Delta_f G^o_m(T) &= 4\,\Delta_f G^o_m(Na^+, aq, T) + 3\,\Delta_f G^o_m(H_2O, l, T),\\ &\quad - 6\Delta_f G^o_m(H^+, aq, T),\\ &\quad + \Delta_f G^o_m(MO_2^{2+}, aq, T) - \Delta_f G^o_m(Na_4MO_5, cr, T), \quad (8)\\ &= f(T) + \Delta_f G^o_m(MO_2^{2+}, aq, T) - \Delta_f G^o_m(Na_4MO_5, cr, T). \quad (9)\end{aligned}$$

The Gibbs energies of formation of the species Na_4MO_5 and MO_2^{2+} are the only terms that differ in between the expressions of the dissociation energies of the sodium uranate and neptunate compounds. The other terms can be expressed as $f(T)$, independent of the actinide cation. The Gibbs energies of formation of the uranium and neptunium aqua ions were reported at T = 298.15 K as −(952.551 ± 1.747) kJ · mol^{-1} and −(795.939 ± 5.615) kJ · mol^{-1} [15], respectively. Using the latter values and those tabulated for Na^+(aq), H^+(aq), and H_2O(l) [15], the Gibbs energies of dissociation are derived at T = 298.15 K as −(410.1 ± 3.4) kJ · mol^{-1} and −(395.5 ± 8.2) kJ · mol^{-1} for Na_4UO_5 and Na_4NpO_5, respectively. The sodium neptunate appears slightly more stable than the sodium uranate, even if the difference remains small considering the uncertainty ranges.

5. Conclusions

The heat capacities of Na_4UO_5 and Na_4NpO_5 have been measured over the temperature range (1.9 to 292) K using a

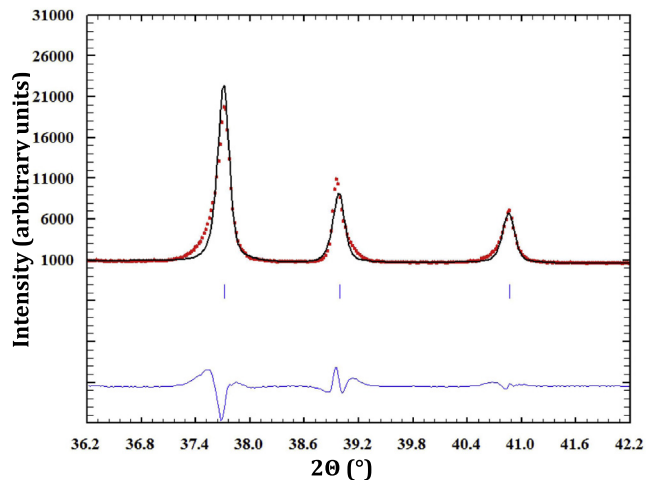

FIGURE 6. Zoom of the X-ray diffraction pattern of Na_4NpO_5 at low angles showing the asymmetric profile in opposite directions for successive *hkl* reflections, which is particularly pronounced at low angles. This is due to slight heterogeneity within the material which creates stresses. Figure taken from [13].

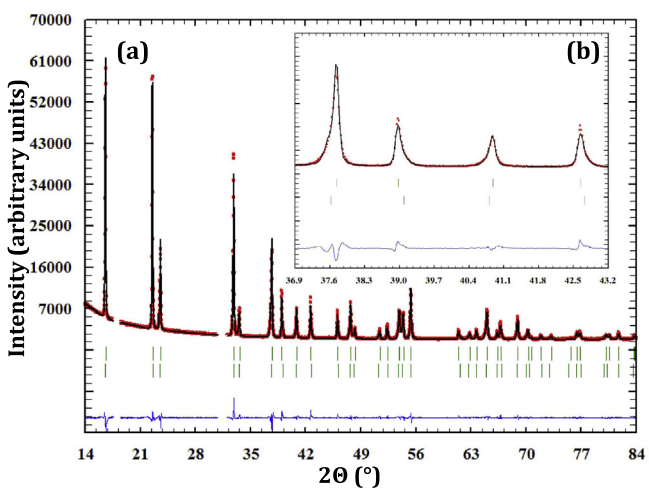

FIGURE 7. (a) Comparison between the observed (Y_{obs}, in red) and calculated (Y_{calc}, in black) X-ray diffraction patterns of Na_4NpO_5. Y_{obs}-Y_{calc}, in blue, is the difference between the experimental and calculated intensities. The Bragg reflections' angular positions are marked in green. Measurement at λ = Cu − Kα1. (b) The inset shows a zoom between 36.9 and 43.2°. (For interpretation of the references to color in this figure legend, the reader is referred to the web version of this article.)

Quantum Design PPMS calorimeter. The experimental data have been fitted using theoretical functions below T = (20.0 and 4.3) K, respectively, and a combination of one Debye and two Einstein functions above T = (20.0 and 23.2) K, respectively. The theoretical fitting required the use of a linear term for the neptunium compound, which could be related to the presence of a non negligible amount of defects, in good agreement with the peak profile shape of the corresponding X-ray diffraction pattern. A broad Schotkky anomaly has also been observed between T = (3 and 15) K, which is associated with two low-lying electronic energy levels separated by about (14 to 16) cm^{-1} (see tables 1–3).

The fitting functions have been used to derive the heat capacities and entropies of both compounds at T = 298.15 K. Combining the data with the enthalpies of formation reported in the literature, the Gibbs energies of formation have finally been determined, and are listed in table 5. Comparing the Gibbs energy values, the sodium neptunate was found to be slightly more stable than its isostructural uranium analogue.

Acknowledgments

The authors would like to express their gratitude to D. Bouëxière for the collection of X-ray data, and to the Analytical Services of the Institute for Transuranium Elements for performing the ICP-MS analysis. They also thank the 7th Framework Program of the European Commission, and the Joint Advanced Severe Accidents Modelling and Integration for Na-cooled neutron reactors (JASMIN) programme (N°295803 in FP7). ALS acknowledges the European Commission and the Ras al Khaimah Centre for Advanced Materials for funding her PhD studentship. ALS also thanks Prof. A. K. Cheetham from the Department of Materials Science and Metallurgy of the University of Cambridge for the fruitful discussions, and his strong and continuous support.

Appendix A

The X-ray diffraction pattern of the synthesized Na_4NpO_5 material showed Bragg reflections with an asymmetric peak profile shape in opposite directions for successive *hkl* reflections, as reported in our previous work [13]. This effect is particularly pronounced at low angles. figure 6, which is taken from [13], illustrates this feature between 2θ = 36.2 to 42.2°. This effect was related to slight heterogeneity within the material, which creates stresses [13].

The fitting of the low temperature heat capacity data reported herein at low temperatures (T < 4.3 K) required the addition of a linear term to describe the experimental curve. The existence of an electronic contribution is ruled out, however, as Na_4NpO_5 is a lime-green insulating material. But the work of [27] suggested that such a linear term could arise due to departure from stoichiometry, oxygen vacancies, or defects within an insulating material. It is therefore suggested that the Na_4NpO_5 material shows oxygen vacancies or defects.

It was subsequently attempted in the present work to introduce a second tetragonal phase, in space group $I4/m$, to improve the Rietveld refinement of the experimental X-ray diffraction data. The refinement was constrained, however, with respect to a number of parameters: both tetragonal phases were forced to adopt the same atomic positional, asymmetry, and peak shape η parameters. In fact, only the cell parameters were allowed to differ from one phase to the other. The corresponding refinement is shown in figure 7. As can be seen in the latter figure, this approach allows a much better description of the peak profile shape, which is also reflected in the value of the R_{wp} factor reduced to 11.2% (as opposed to 17.7% when performing the refinement with a single tetragonal phase [13]) (table 6). The refined bond lengths, listed in table 7, are very close to the ones reported previously [13].

The refined cell parameters are found as (a = 0.7532(3) nm, c = 0.4618(3) nm) and (a = 0.7555(3) nm, c = 0.4605(3) nm) for the first and second tetragonal phases, respectively, the corresponding weight fractions being 61.8 wt% and 38.2 wt%. This yields unit cell volumes of 0.2620(2) and 0.2628(2) nm^3, respectively. The second phase showing a larger cell volume could correspond to the defect fraction of the material. Its rather large weight fraction (38.2 wt%) causes a similarly large linear δT contribution ($\sim$275 $mJ \cdot K^{-2} \cdot mol^{-1}$) below T = 4.3 K in the experimental heat capacity data.

References

[1] L. Koch, J. Less-Common Met. 122 (1986) 371–382.
[2] C.T. Walker, G. Nicolaou, J. Nucl. Mater. 218 (1995) 129–138.
[3] E.H.P. Cordfunke, D.J.W. IJdo, J. Solid State Chem. 115 (1995) 299–304.
[4] S. Pillon, F. Ingold, P. Fischer, G. Andre, F. Botta, R.W. Stratton, J. Nucl. Mater. 206 (1993) 50–56.
[5] I.P. Roof, M.D. Smith, H.-C. zur Loye, J. Cryst. Growth 312 (2010) 1240–1243.

[6] S. Van den Berghe, A. Leenaers, C. Ritter, J. Solid State Chem. 177 (2004) 2231–2236.
[7] A.L. Smith, P.E. Raison, L. Martel, T. Charpentier, I. Farnan, D. Prieur, C. Hennig, A. Scheinost, R.J.M. Konings, A.K. Cheetham, Inorg. Chem. 53 (1) (2014) 375–382.
[8] A.L. Smith, P.E. Raison, L. Martel, D. Prieur, T. Charpentier, G. Wallez, E. Suard, A.C. Scheinost, C. Hennig, P. Martin, K.O. Kvashnina, A.K. Cheetham, R.J.M. Konings, Inorg. Chem. 54 (7) (2015) 3552–3561.
[9] C. Keller, L. Koch, K.H. Walter, J. Inorg. Nucl. Chem. 27 (1965) 1205–1223.
[10] C. Keller, L. Koch, K.H. Walter, J. Inorg. Nucl. Chem. 27 (1965) 1225–1232.
[11] A.L. Smith, P.E. Raison, R.J.M. Konings, J. Nucl. Mater. 413 (2011) 114–121.
[12] D. Bykov, P. Raison, R.J.M. Konings, C. Apostolidis, M. Orlova, J. Nucl. Mater. 457 (2015) 54–62.
[13] A.L. Smith, A. Hen, P.E. Raison, E. Colineau, J.-C. Griveau, N. Magnani, J.P. Sanchez, R.J.M. Konings, R. Caciuffo, A.K. Cheetham, Inorg. Chem. 54 (9) (2015) 4556–4564.
[14] I. Grenthe, J. Fuger, R.J.M. Konings, R.J. Lemire, A.B. Muller, C. Nguyen-Trung Cregu, H. Wanner, Chemical thermodynamics of uranium. OECD Nuclear Energy Agency, Data Bank, Issy-les-Moulineaux, France, 1992.
[15] R. Guillaumont, T. Fanghänel, J. Fuger, I. Grenthe, V. Neck, D.A. Palmer, M.H. Rand, Update on the chemical thermodynamics of uranium, neptunium, plutonium, americium & technetium, OECD Nuclear Energy Agency, Data Bank Issy-les-Moulineaux, France, 2003.
[16] C. Keller, in: K.W. Bagnall (Ed.), Inorg. Chem., Ser. 1, 7, Butterworths, London, 1972, p. 479.
[17] S. Pillon, Etude des diagrammes de phases U–O–Na, Pu–O–Na et U, Pu–O–Na (PhD thesis), Université Du Languedoc, 1989.
[18] H. Kleykamp, KfK 4701 (1990) 31.
[19] J. Goudiakas, X. Jemine, J. Fuger, J. Chem. Thermodyn. 23 (1991) 513–520.
[20] J. Fuger, J. Nucl. Mater. 130 (1985) 253–265.
[21] A.L. Smith, J.-Y. Colle, O. Beneš, A. Kovacs, P.E. Raison, R.J.M. Konings, J. Chem. Thermodyn. 60 (2013) 132–141.
[22] J. Rodriguez-Carvajal, Physica B 192 (1993) 55–69.
[23] J.C. Lashley, M.F. Hundley, A. Migliori, J.L. Sarrao, P.G. Pagliuso, T.W. Darling, M. Jaime, J.C. Cooley, W.L. Hults, L. Morales, D.J. Thoma, J.L. Smith, J. Boerio-Goates, B.F. Woodfield, G.R. Stewart, R.A. Fisher, N.E. Phillips, Cryogenics 43 (6) (2003) 369–378.
[24] P. Javorský, F. Wastin, E. Colineau, J. Rebizant, P. Boulet, G. Stewart, J. Nucl. Mater. 344 (1–3) (2005) 50–55.
[25] D.W. Osborne, H.E. Flotow, R.P. Dallinger, H.R. Hoekstra, J. Chem. Thermodyn. 6 (1974) 751–756.
[26] A.L. Smith, J.-C. Griveau, E. Colineau, P. Raison, R.J.M. Konings, Thermochim. Acta (2015). submitted.
[27] J. Majzlan, A. Navrotsky, B.F. Woodfield, B.E. Lang, J. Boerio-Goates, R.A. Fisher, J. Low Temp. Phys. 130 (1–2) (2003) 69–76.
[28] B.F. Woodfield, J. Boerio-Goates, J.L. Shapiro, R.L. Putnam, A. Navrotsky, J. Chem. Thermodyn. 31 (1999) 245–253.
[29] B.F. Woodfield, J.L. Shapiro, R. Stevens, J. Boerio-Goates, R.L. Putnam, K.B. Helean, A. Navrotsky, J. Chem. Thermodyn. 31 (1999) 1573–1583.
[30] S.J. Smith, R. Stevens, S. Liu, G. Li, A. Navrotsky, J. Boerio-Goates, B.F. Woodfield, Am. Miner. 94 (2009) 236–243.
[31] R.A. Swalin, Thermodynamics of Solids, first edition., John Wiley & Sons, 1962.
[32] R.D. Shannon, Acta Cryst. A32 (1976) 751–767.
[33] Q. Shi, T.-J. Park, J. Schliesser, A. Navrotsky, B.F. Woodfield, J. Chem. Thermodyn. 72 (2014) 77–84.
[34] E.S. Gopal, Specific Heats at Low Temperatures, Plenum Press, New York, 1966.
[35] Q. Shi, L. Zhang, M.E. Schlesinger, J. Boerio-Goates, B.F. Woodfield, J. Chem. Thermodyn. 6 (2013) 51–57.
[36] J. Leitner, P. Voňka, D. Sedmidubský, P. Svoboda, Thermochim. Acta 497 (2010) 7–13.
[37] R.J.M. Konings, O. Beneš, J. Phys. Chem. Ref. Data 39 (2010) 043102.
[38] M.W. Chase, Nist-JANAF Thermochemical Tables, 4th edition., American Chemical Society, American Institute of Physics, National Bureau of Standarts, New York, 1998.
[39] I. Ansara, B. Sundman, Scientific Group Thermodata Europe, Computer Handling and Determination of Data, North Holland, Amsterdam, 1986.

JCT 15-194